International Journal of Mass Spectrometry 290 (2010) 47–59

Contents lists available at ScienceDirect

International Journal of Mass Spectrometry

journal homepage: www.elsevier.com/locate/ijms

Surface-assisted laser desorption/ionization mass spectrometry on nanostructured silicon substrates prepared by iodine-assisted etching

K.P. Law*

Centre for Analytical Bioscience, and Laboratory of Biophysics and Surface Analysis, School of Pharmacy, University of Nottingham, Nottingham, UK

ARTICLE INFO

Article history:
Received 15 August 2009
Received in revised form
22 November 2009
Accepted 3 December 2009
Available online 17 December 2009

Keywords:
Surface-assisted laser desorption/ionization mass spectrometry
Surface analysis
Surface imaging
Ionization mechanism

ABSTRACT

Surface-assisted laser desorption/ionization (SALDI) is a matrix-free mass spectrometry (MS) approach that utilizes the unique properties of a nanostructured surface to promote desorption and ionization. However, there are still questions on what constitutes a suitable SALDI substrate for mass spectrometric application. A range of SALDI substrates prepared by anodization with an oxidizing electrolyte was investigated. The laser desorption/ionization (LDI) performance was examined on a reflectron time-of-flight (ToF) mass spectrometer. The physicochemical properties of the substrates were characterized by a number of surface analysis techniques including scanning electron microscopy (SEM), atomic force microscopy (AFM), secondary ion mass spectrometry (SIMS), X-ray photoelectron spectroscopy (XPS) and water contact angle measurement. Examination of surface cleaning technologies and methods for surface chemical modification were carried out. Correlation between the substrate physicochemical properties and the LDI performance was determined. It was found that only the substrate, which had a thick nanostructured layer, was effective for LDI-MS. SALDI substrate was found to have a high surface potential. However, this unique property offered no advantage for the application of LDI-MS. Surface chemistry is also an important factor in affecting the LDI performance. Plasma etching can effectively remove the surface contamination but it also increases the thickness of the oxide layer. Fluorine and hydroxyl termination is advantageous. Fluorine passivation increases the surface hydrophobicity, which confines the analyte solution droplet to a smaller area and also withdraws the electronic density from the surface, and acidifies the surface Si–OH moieties, which is believed a major proton source. The effect of laser etching was investigated by SIMS and XPS imaging and provided new insight of the SALDI ionization mechanism.

1. Introduction

Matrix-assisted laser desorption/ionization (MALDI) has revolutionized biochemical mass spectrometry and is an indispensable tool in proteomics and macromolecules mass analysis [1,2]. Despite the success of MALDI, one major drawback of the technique is that the mass spectra have a high chemical background due to the formation of clusters of matrix ions or the degradation products of the matrix. Generally, for organic matrices, the matrix interference occurs at the low mass region (m/z 700 and below) of the spectra. Because of this matrix interference, the applicability of the MALDI method for small molecule analysis is very limited.

In advancing the MALDI technique, approaches that employ a non-conventional matrix have emerged and these methods are referred to as surface-assisted laser desorption/ionization (SALDI) [3–5]. The attraction of the SALDI approach is the absence of matrix interference in the low mass region of the mass spectra and thus SALDI permits rapid analysis of small molecules. The SALDI technique was originally developed by Sunner and Chen as early as 1995 [6]. A mixture of carbon powder and glycerol was initially the substrate of choice. Since then a number of different materials that can serve as SALDI matrices have been proposed [7–9]. A noticeable example was a method termed desorption/ionization on silicon mass spectrometry (DIOS-MS) and was first reported by Wei et al. in 1999 [10]. The method uses pulsed laser desorption/ionization (LDI) on porous silicon (PSi).

The conventional method for the PSi preparation involves electrochemical etching of crystalline silicon using aqueous HF electrolyte and the resulting material has a morphology composed by a disordered web of pores entering into Si. Its structure is like a sponge where quantum effects play a fundamental role. These features, being a quantum system and a sponge are keys both to the success and failure of PSi [11]. Some believe that the conventional method in preparing the PSi material has limited the full poten-

* Present address: Clinical Sciences Research Institute,Warwick Medical School, University of Warwick, University Hospital, Clifford Bridge Road, Coventry, CV2 2DX, UK. Tel.: +44 24 7696 8634.
E-mail address: k.law@warwick.ac.uk.

1387-3806/$ – see front matter © 2009 Elsevier B.V. All rights reserved.
doi:10.1016/j.ijms.2009.12.003

tial of the material for the application of SALDI-MS. An alternative method is to use stain etching. This method involves an addition of an oxidising agent into an aqueous HF electrolyte [12]. Nitric acid is an oxidising agent commonly used. Other examples include H_3PO_4 [13], and CrO_4 [14]. Stain etching simplifies the preparation procedures by either removing light illumination or electrical bias. Stain etching is also useful if one needs to produce a very thin PSi film. Recently, it was reported that the PSi substrates prepared by stain etching using iodine-containing electrolyte were suitable for the GC/SALDI-MS application [15,16]. Relatively, iodine is a very weak oxidizer, and consequently the iodine in ethanol solution leads to little direct chemical etching. It was suggested that this preparation method leads to a long-term stabilization of both the photoluminescent properties and the surface states [17,18].

However, information related to the physicochemical properties of these SALDI substrates is still unavailable and the effect of the laser modification remains unclear despite a theory having been proposed. Most important of all, are these SALDI substrates suitable for the conventional liquid deposition or dry droplet approach and can they be used for the analysis of complex biological matrix? In-line with the previous reports, these have been investigated in this study. In addition, experiments on surface cleaning technologies and chemical derivatization to enhance the usability and performance of the SALDI substrates have also been carried out.

2. Experimental

2.1. Materials

Deionized water (18 MΩ) was generated by a USF Elga (Stoke-on-Trent, UK) Maxima water purification system. Gradient grade acetonitrile, HPLC grade methanol, isopropanol, formic acid and trifluoroacetic acid were purchased from Fisher (Loughborough, UK). 2-(4-Aminophenyl)-6-methylbenzothiazole, alprenolol hydrochloride, labetalol hydrochloride, procainamide hydrochloride, ethylenediamine, nadolol, metoprolol tartrate, timolol maleate, folinic acid, nalidixic acid and biochemical grade vitamin B_{12} were purchased from Sigma–Aldrich (Poole, UK). Atenolol was purchased from MP Biomedicals (Illkirch, France) and Human angiotensin I was purchased from Calbiochem (Nottingham, UK).

2.2. SALDI substrates

The substrates for the investigation were prepared and supplied by Vladimir Karavanskii, of A.M. Prokhorov General Physics Institute, Moscow, Russia. The samples were prepared by a patented anodization technique on crystalline silicon using iodine-containing electrolytes [19,20]. It was demonstrated in [15] that this fabrication procedure produced substrates that are effective for GC/SALDI mass spectrometry and have a long-term stability.

2.3. Argon plasma etching

Plasma etching was carried out in a Bio-Rad (Hemel Hempstead, UK) RF Plasma Barrel Etcher PT7100 operated using auto reflected power mode. Samples were stored in isopropanol and dried on a Petri dish before placing into the etching chamber. Etching was carried out using ~3 Pa argon gas, forward power was ~40 W and reflected power ~3 W. Samples were immersed immediately in isopropanol after etching and stored until analysis.

2.4. Fluorosilane self-assembly monolayer (SAM) modification

The sample was first cleaned using argon plasma etching. Immediately after plasma treatment, the sample was placed inside a custom built reaction vessel and was allowed to react with 2% (w/v) of 1H,1H,2H,2H-perfluorodecyldimethylchlorosilane (Lancaster, Heysham, UK) in AR grade toluene (Fisher) at 90–110 °C for an hour.

2.5. Surface imaging and topography analysis by scanning electron microscopy (SEM) and atomic force microscopy (AFM)

SEM analysis was carried out in high vacuum mode using a JEOL (Tokyo, Japan) JSM-6060LV SEM instrument. No gold coating was required. AFM investigation was carried out on a MultiMode AFM or Dimension 3100 Scanning Probe Microscope (SPM) (Veeco, Santa Barbra, CA, USA) operated using a single laser beam under tapping-mode with an etched silicon probe tip (TESP). Acquired images were analysed using Image Metrology SPIP Version 4.

2.6. Time-of-flight secondary ion mass spectrometry (ToF-SIMS)

SIMS analysis was performed with a TOF-SIMS IV instrument (ION-TOF GmbH, Münster, Germany). The instrument employed a 15 keV $^{69}Ga^+$ liquid metal ion gun (LMIG) with 10 kV post-acceleration and a single-stage reflectron analyser. The AC primary ion (PI) beam was pulsed at 10 kHz frequency using a current between 1.06 and 1.17 pA for Ga^+ LMIG, bombarding an area from 100 μm × 100 μm (for high mass resolution) to 500 μm × 500 μm (for high sensitivity). Both positive and negative ion spectra were acquired for each analysis area, with an ion dose of 5×10^{11} PI/cm^2 per polarity. Optical images were also taken. SIMS ion mapping was achieved by rastering an area of 500 μm × 500 μm under the pulsed PI beam, using a raster of 512 × 512 pixels. Calibration of the mass spectra in the positive detection mode was based on the following peaks, CH_2^+ (14.0157 amu), $C_2H_2^+$ (26.0157 amu), $C_3H_2^+$ (38.0157 amu), and $C_4H_3^+$ (51.0235 amu); and in negative detection mode on CH_2^- (14.0157 amu), C_2^- (24.0000 amu), C_3^- (36.0000 amu), and C_4H^- (49.0078 amu). Data acquisition and post-processing analyses were performed using IonSpec Version 4.010 and IonImage Version 4.0.

2.7. X-ray photoelectron spectroscopy (XPS)

XPS was carried out on a Kratos AXIS Ultra (Kratos Analytical Ltd., Manchester, UK) instrument, using a monochromatic beam from an aluminium source run at 150 W. A take-off angle of 90° was used, and the samples were analysed with the charge neutraliser on. The survey and core-level spectra were collected using a pass energy of 80 eV and 20 eV, respectively. The photoelectron images were taken using the spherical mirror analyser from an area of 800 μm × 800 μm with 256 × 256 pixels, the multi-spectral datasets being acquired at 40 eV pass energy, with field of view at 1, image aperture at 1 and stepping through the chosen energy regions at 0.2 eV intervals. Datafiles were collected using the instrument Vision 2 software and processed using CasaXPS version 2.3.1.2 with Kratos sensitivity factors. The spectra were corrected to position the C–C within the C 1s core-level at a binding energy (BE) of 285.0 eV.

2.8. Water contact angle (WCA) measurement

WCA measurements were carried out using a KSV (Helsinki, Finland) CAM 200 system equipped with manual liquid dispenser, and a high-speed digital CCD fire-wire camera and LED based stroboscope. Deionized water was used as the test liquid. The measurements were carried out at room temperature.

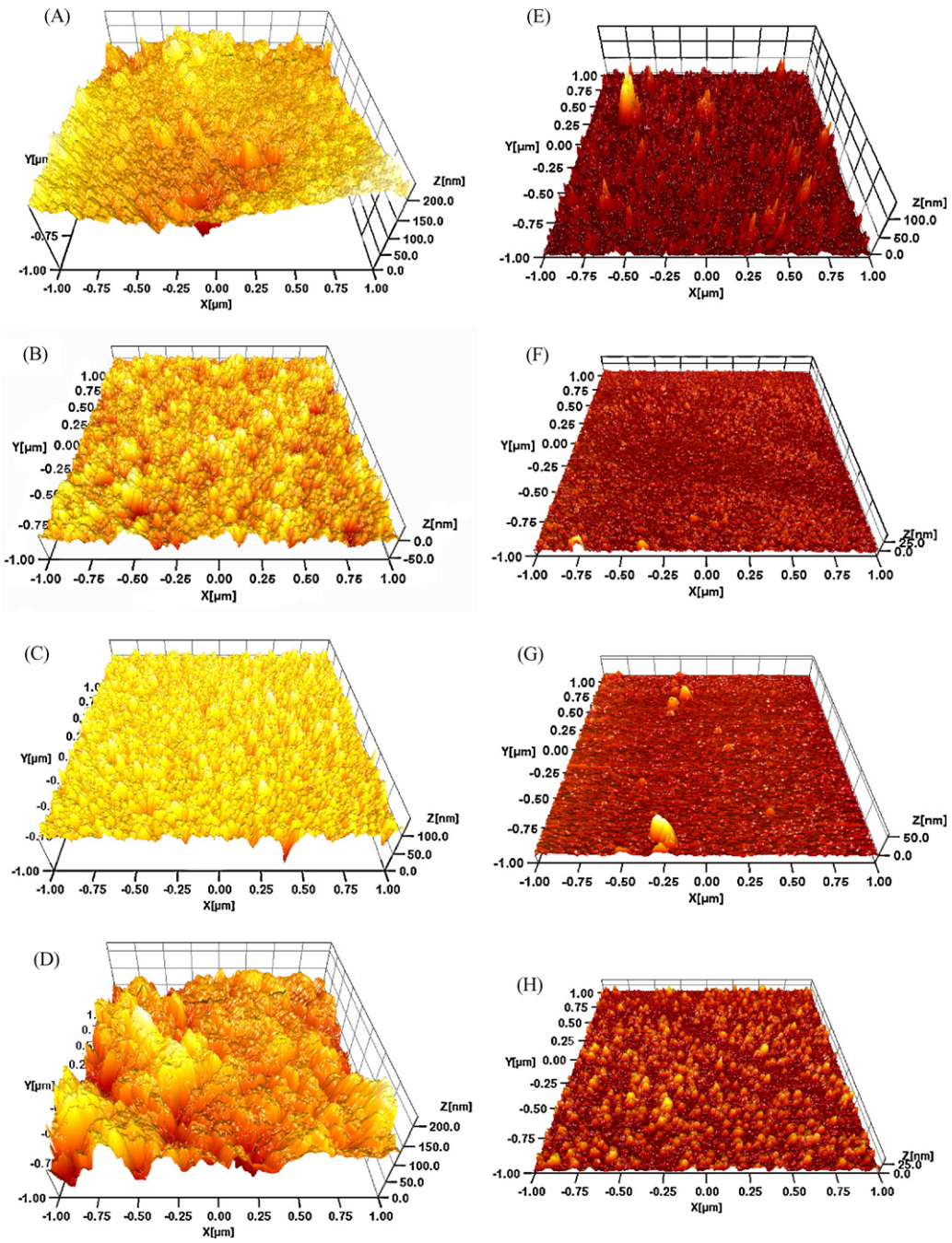

Fig. 1. AFM images of eight representative SALDI substrates and are labeled as S1–S8. (A) S1, (B) S2, (C) S3, (D) S4, (E) S5, (F) S6, (G) S7 and (H) S8. Surface roughness measured by AFM in root mean square was 23.2, 10.6, 10.0, 26.9, 9.41, 2.67, 3.60 and 4.57 nm, respectively.

2.9. Laser mass spectrometry

Surface handling and analyte solution deposition were carried out in a laminar flow-hood to minimise atmospheric contamination. SALDI substrates were cleaved to suitable size and mounted onto a modified steel plate using double-sided conductive tape. Analyte solution was deposited onto the target surface using a pipette. Analyte solution was prepared in 50% acetonitrile. Unless stated otherwise, 1 μL of solution was added on each well and air-dried.

Mass spectra were acquired using a Micromass (Manchester, UK) M@LDI-TOF mass spectrometer operating in reflectron mode. Pulse voltage was 3500 V. Delay time extraction was 500 ns. The laser energy was set to a constant value. Spectra were acquired at 5 Hz using a nitrogen laser (337 nm). Data acquisition and post-processing analyses were performed using MassLynx Version 4.0. All data was acquired in positive ion mode.

3. Results and discussion

3.1. Surface morphology analysis and the LDI performance

The surface morphology is believed to play a crucial role in the LDI performance and hence the substrates were investigated by AFM and SEM. Eight representative SALDI substrates are chosen to present here and their AFM images are shown in Fig. 1. The substrates were prepared by varing the etching current, etching time and the concentration of iodine. A wide range of nanostruc-

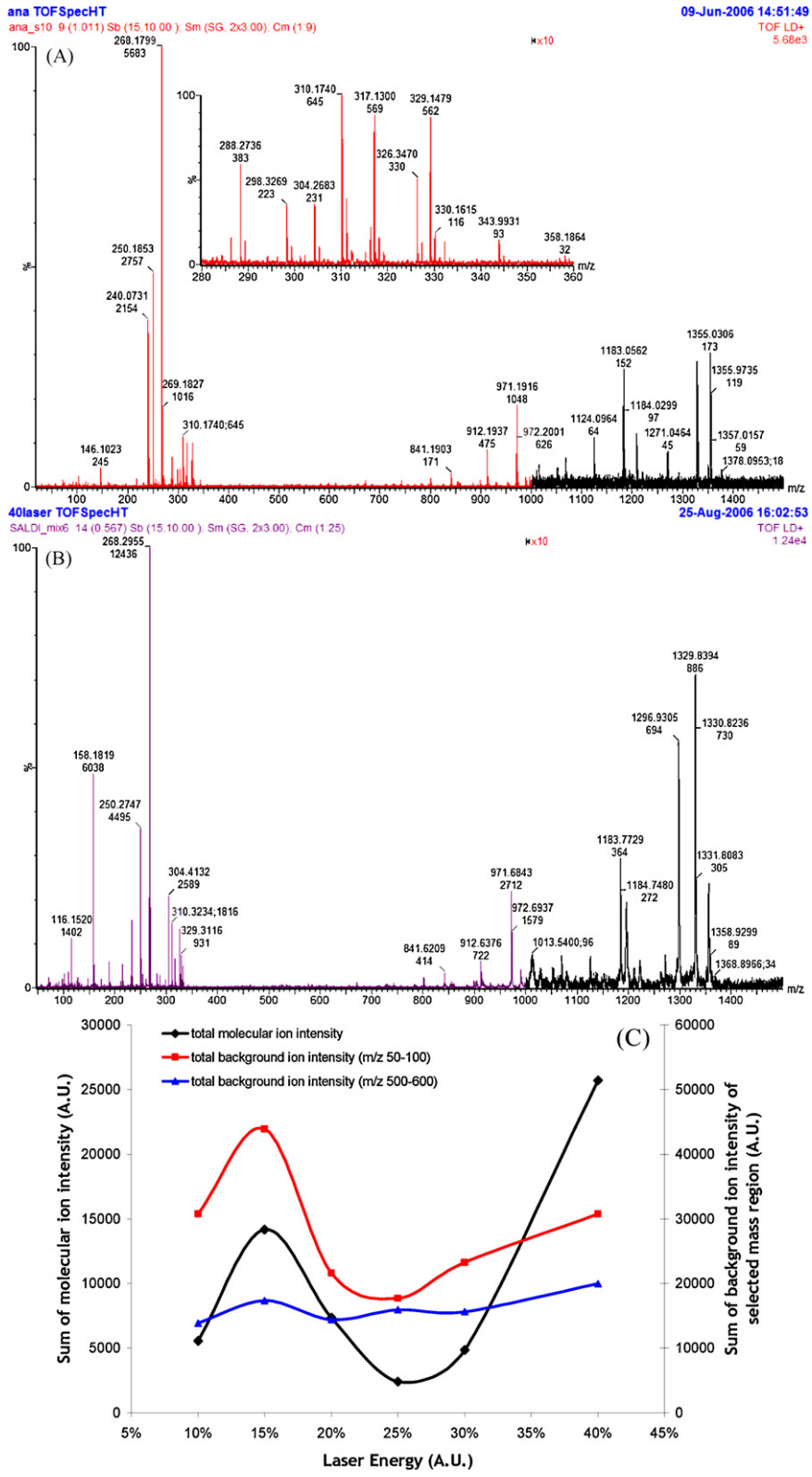

Fig. 2. (A) Positive ion SALDI mass spectrum of a mixture containing 8-hydroxyquinoline ([M+H]$^+$ at m/z 146), 2-(4-aminophenyl)-6-methylbenzothiazole ([M]$^+$ at m/z 240), alprenolol ([M+H]$^+$ at m/z 250), atenolol ([M+H]$^+$ at m/z 267), metoprolol ([M+H]$^+$ at m/z 268), nadolol ([M+H]$^+$ at m/z 310), timolol ([M+H]$^+$ at m/z 317), labetaol ([M+H]$^+$ at m/z 329) and vitamin B_{12} ([M+H]$^+$ at m/z 1355). The spectrum was acquired using the substrate S1 and the substrate had been stored for 8 month in isopropanol and was sonicated 10–15 s to remove surface contamination. Insert displays a magnified region between m/z 280–360. (B) Positive ion SALDI mass spectrum of a mixture containing nalidixic acid ([M+H]$^+$ at m/z 233), alprenolol ([M+H]$^+$ at m/z 250), atenolol ([M+H]$^+$ at m/z 267), metoprolol 392 ([M+H]$^+$ at m/z 268), nadolol ([M+H]$^+$ at m/z 310), timolol ([M+H]$^+$ at m/z 317), labetalol ([M+H]$^+$ at m/z 329), angiotensin I ([M+H]$^+$ at m/z 1296.5), vitamin B_{12} ([M+H]$^+$ at m/z 1355.5), folinic acid and erythromycin. Folinic acid and erythromycin were not detected as protonated ion. The spectrum was acquired using the substrate S2. The mass spectrum presented was acquired with laser energy setting 40%. (C) The total signal intensity of the molecular ions and background ions of two-selected mass regions (m/z 50–100 and m/z 500–600) as a function of laser energy setting of the instrument.

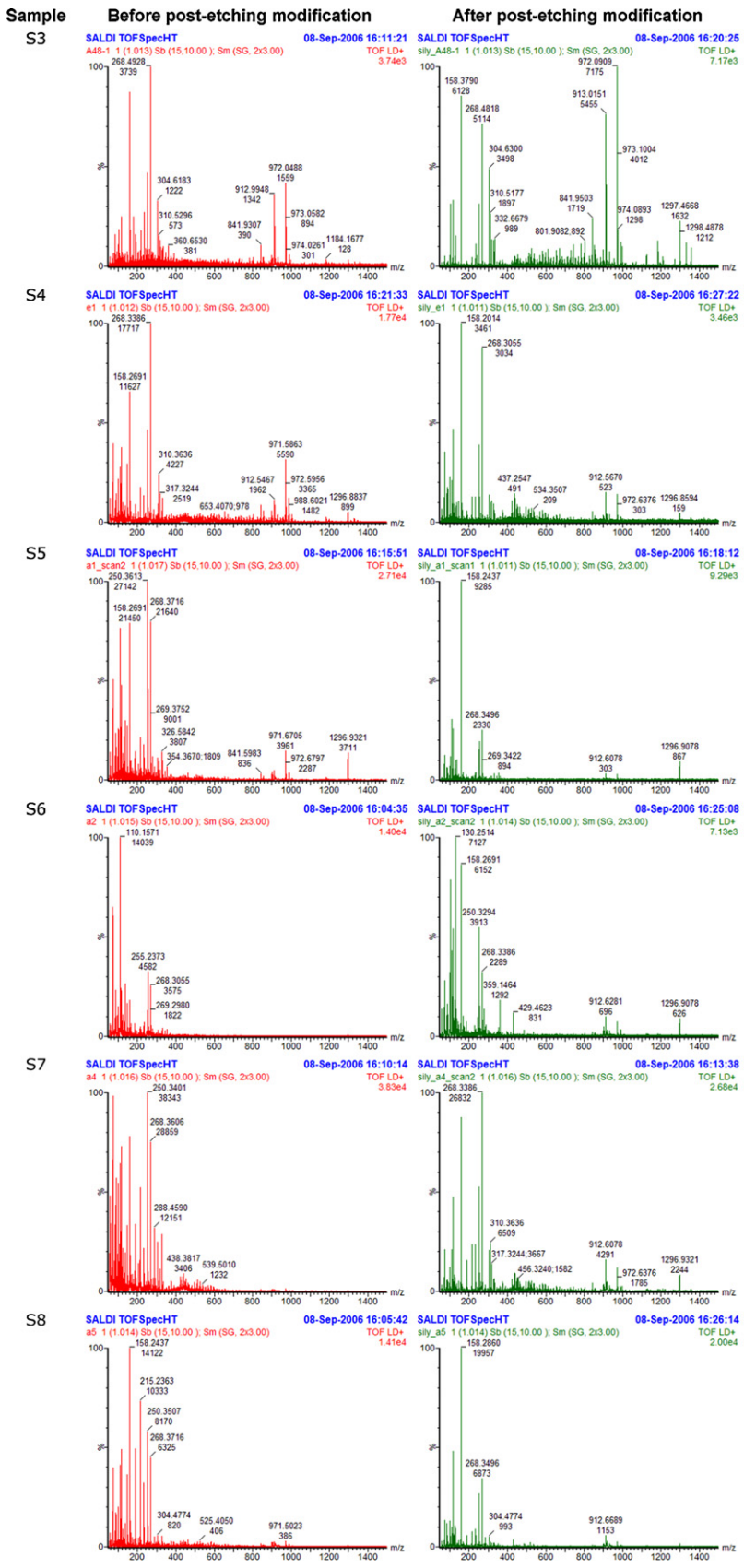

Fig. 3. Positive ion SALDI mass spectra of the as-received and fluoro-silanised SALDI substrates, S3–S8. Spectra were acquired using the mixture as in Fig. 2B. The mass spectra were acquired with laser energy setting 10%.

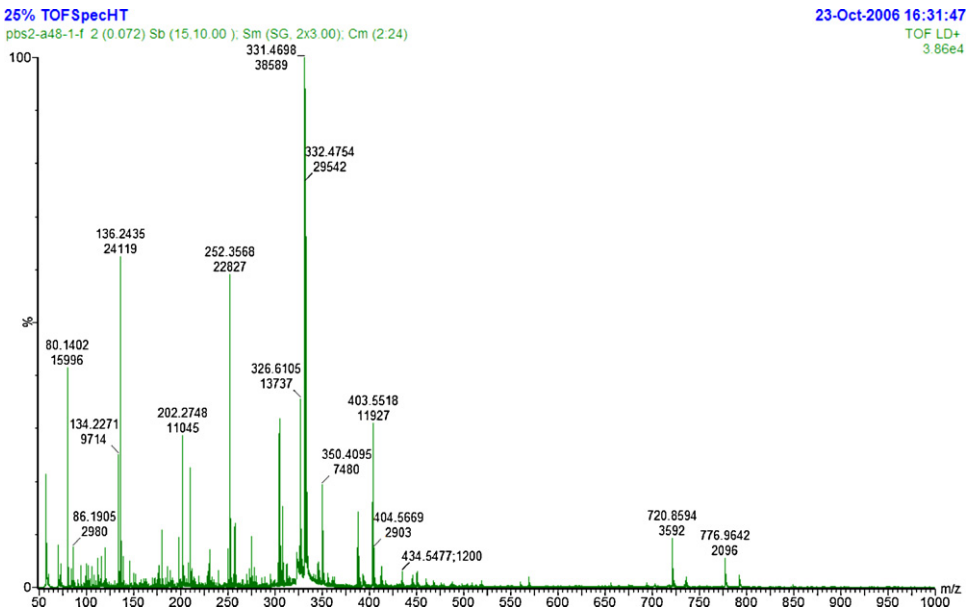

Fig. 4. A representative positive ion SALDI mass spectrum of a bacterial extract. The spectrum was acquired using modified substrate S3.

tured surface morphology could be obtained. The substrates were classified as two major types here: (1) those that have a thick roughened or porous layer (substrates S1–S4) and (2) those are relatively smooth, of which the surface roughness measured by AFM has only a few nm (substrates S5–S8).

Substrate S1 exhibited a non-conventional surface morphology. Additional optical and SEM images are presented in the supplementary material (Fig. S-1A and B) to illustrate the surface morphology at different magnification. The substrate was prepared by a two-step etching procedure. The substrate had dents of curvature and this appeared formed because of bubble formation during etching. The nanostructures observed in the AFM image were produced by the second etching. Although this substrate was ineffective for the GC/SALDI-MS approach, it gave a good quality SALDI mass spectrum using the liquid deposition approach, for both small and larger molecules (Fig. 2A). The spectrum was acquired with a laser energy setting within the normal range for the conventional matrix MALDI technique and had a good signal-to-noise ratio. Given that the substrate was non-porous, this implies that pores are not a strict requirement for the SALDI-MS but the high density of surface nanostructures is. Furthermore, the stability of this substrate is demonstrated. The mass spectrum was acquired 8 months after the substrate was prepared and it had only been stored in solvent since.

On the other hand, substrates S2 and S3 (Fig. 1B and C) were porous and the substrates had a thick porous layer. The thickness of the porous layer measured by AFM was 100 and 150 nm, respectively. The surface roughness measured was about 10 nm in root mean square. Pore opening as shown by SEM in Fig. S-1C was 10–20 nm in diameter and the porosity was relatively low. These two substrates were prepared by the same etching parameters but the silicon substrates differed in their crystal orientation (1 0 0 and 1 1 1, respectively). These led to a different etching rate and a subtle difference in their surface morphology. These two substrates also produced good quality mass spectra and had a similar LDI performance. This suggests that although the crystal orientation affects the rate of chemical etching, this is not an important factor in affecting the SALDI activity. A similar observation was also reported with the DIOS substrate [21,22].

The variation of the ion counts of the protonated ions as a function of the laser energy setting is plotted in Fig. 2C. A maximium was observed at the laser energy of 15% and then the ion intensity dropped and then rose again. At 40%, the ion count exceeded that obtained at 15%. Possibly, there would be another maximum before the laser threshold of surface destruction [23]. This pattern was thought to be related to two closely related but independent energy transfer processes of the SALDI mechanism. At the lower laser energy, the electronic process is the dominant process. As the laser energy is increased higher than 15%, the laser radiation ablates part of the silicon nanoclasters from the surface and changes the surface chemistry. This process disrupts the electronic process and thus the total ion intensity (including contaminant ions) decreases. As the laser energy is increased further, the thermal reaction becomes more important. The surface nanocrystals undergo melting and recrystallization. This process changes the surface nanostructures and induces surface reconfiguration, which leads to increase in the total ion intensity. Ultimately the intense heat induced by the laser radiation would lead to surface destruction. Evidence that in part supports the surface reconfiguation under the influence of laser radiation is presented with the results of SIMS and XPS imaging and will be further elaborated using commerial DIOS^{TM} substarte in the next article.

The variation of the sum of the background ion intensity of two-selected mass regions (m/z 50–100 and m/z 500–600) as a function of the laser energy setting is also plotted in Fig. 2C. The mass region m/z 50–100 of the SALDI spectra contained contaminant ions, which were originated from the manufacturing process, atmospheric species absorbed and/or sample solvent used. The mass region m/z 500–600 of the spectra is also selected because this region was free from any contaminant ion and molecular and fragment ion from the analyte despotised on the surface. This region therefore shows the variation of chemical and random noise (scattered ions). The variation of the sum of background ion intensity in the region m/z 50–100 was strikingly similar to the variation of the sum of molecular ion intensity of the analyte, and hence the LDI of the contaminants had no difference from the LDI of the analyte added. However, the variation of the chemical background of the mass spectra was relatively insensitive to the variation of the laser energy and in the region m/z 500–600, the background level remained approximately a constant throghout the energy range of investigation. High back-

Table 1
Atomic concentration and surface carbonaceous species concentration of a representative SALDI substrate before and after argon plasma etching for 100 s.

SALDI sample	Atomic concentration (at%) on the surface on the SALDI surface determined by XPS survey spectra measurements						High-resolution XPS C 1s component fits (%C)	
	O 1s	C 1s	Si 2s	F 1s	I 3d	Traces	CO	CH
As-received surface	31.4	23.4	44.3	0.9	>0.1		8.2	15.2
Plasma treated surface	54.8	6.0	38.4	0.2	≥0.001	Na, Sn	2.4	3.6

ground was only observed when the laser energy had exceeded the energy threshold of surface destruction. This highlights a unique property of using PSi as a SALDI platfom. This will be further illustrated using the commerial DIOS^{TM} substarte in the next article.

3.2. Post-etching cleaning and modification

Unfortunately, most of the SALDI substrates received suffered surface contamination complication severely and produced strong background interferences in the mass spectra that completely obscured the analyte ion in the low mass region and suppressed the ionization of larger molecules. Although it was suggested that the SALDI substrates could be stored in air for up to a year without any significant decrease in ionization efficiency, without a proper pre-etching precaution and post-etching protection during storage and transport, such a difficulty prohibited their efficient use for mass spectrometry application. This complication had been reported in other matrix-free LDI substrate developments [24–26] and hence a post-etching cleaning and modification procedure was devised. This post-etching cleaning and modification involved argon ion plasma etching and chemical derivatization by fluorosilane. Plasma etching had the advantage of avoiding the use of hazardous chemical and the fluorine passivation led to enhancement in LDI performance. As shown in Fig. S-2, some success in removing the background interferences and improvement in mass resolution was achieved with solvent washing and plasma etching. The reason for higher mass resolution has been given in [27]. The results of further chemical derivatization are given in Fig. 3.

After the modification, all substrates showed some degrees of improvement. The porous substrate S3 that already gave a good LDI performance, received further enhancement as a result of the post-etching modification. Enhancement in ion yield, reduction of threshold laser energy and elimination of background interference was obtained. On the other hand, the substrate S4, as shown in Fig. 1D and Fig. S-1D, had a thick fragile spongy porous structure, the enhancement was relatively minor. It appears that the surface nanostructure did not have the mechanical strength to withstand the vigorous procedure and had the nanostructure destroyed. Although the weak mechanical strength of the surface nanostructure was less than ideal, the substrate still gave reasonable quality mass spectra. This was in contrast to the substrate S5–S8, which only had a very thin roughened layer of 10–50 nm thick and gave low quality mass spectra. The spectra suffered strongly from the background interferences at the lower mass region and poor performance at the higher mass region prior to the modification. The largest improvement was obtained on substrate S7 after the modification. The larger molecules became detectable and the level of interference became significantly lower. Overall, no strong correlation between the surface roughness and the LDI performance was found.

It was also further demonstrated that the derivatized substrates could be used for the analysis of complex biological matrix. A SALDI mass spectrum of a bacterial extract derivatized with isobutyl-chloroformate is shown in Fig. 4 using a modified substrate S3.

3.3. Investigation of the surface chemistry and the effect of plasma etching by ToF-SIMS

The SIMS spectra generally showed a high level of hydrocarbon clusters and various silicon hydride and oxide signals. The results are presented along with the effort to clean these substrates by argon plasma etching.

The surface of the SALDI substrates contained a wide range of molecular species. Figs. S-3 and S-4 show the positive and negative ion SIMS spectra of a typical SALDI surface before and after 100 s of argon plasma treatment, respectively. Identical primary ion dose was used to acquire the SIMS spectra. Si^+ (m/z, 28) and O^- (m/z, 16) dominate the positive and the negative SIMS spectra, respectively and their intensities increase after the plasma etching. The positive ion spectra also show that the intensity of SiH^+ (m/z, 29) was reduced, and yet the intensity of $SiHO^+$ (m/z, 45) was increased after the plasma treatment. These suggest that the plasma etching procedure has increased the surface concentration or thickness of the oxide layer. On the other hand, the intensity of Na^+ (m/z, 22.99) was higher after the plasma etching. The ion intensities of hydrocarbon species, *e.g.*, CH_3^+ (m/z, 15) and $C_2H_3^+$ (m/z, 27) were diminished. In addition, a high intensity of I^- ion (m/z, 127) was observed in the negative spectra but the Si–I^- ion was absent. Initially, it was thought the absence of Si–I^- ion was due to the ion instability. Subsequent investigation revealed the I^- ion detected was in the form of iodide salt.

To evaluate the change in surface chemistry due to argon plasma etching, the raw data was converted to Figs. S-5 and S-6, which illustrate the relative change of ion intensities in the SIMS spectra before and after argon plasma etching, in the positive and negative ion spectra, respectively. Most of the organic species detected showed a negative change in their relative intensity and the removal of organic species was achievable by argon plasma etching. The negative ion spectra also showed that the hydrocarbon and halide ions, such as F^-, Cl^- and I^- were removed after the plasma treatment. Furthermore, the surface was oxidized as the secondary ions of various oxides had a relatively higher intensity.

3.4. Investigation of the surface chemistry and the effect of plasma etching by XPS

Figs. S-7 and S-8 show the XPS spectra of a typical SALDI surface before and after 100 s plasma etching, respectively. The prominent peaks were due to silicon, carbon, and oxygen. Small amount of fluorine and iodine were also detected. Table 1 summarizes the quantification of the elemental and carbonaceous species.

After argon plasma etching, the levels of carbon, fluorine, and iodine were significantly reduced. However, the level of oxygen was elevated. Sodium and tin on the SALDI surface became detectable after plasma etching. The core-level O 1s deconvolution suggested that both oxides and hydroxides were increased due to plasma etching, but higher proportion of hydroxides than oxides in this case (Figs. S-7B and S-8B). The core-level C 1s deconvolution showed that only the peaks of CH and CO and these carbonaceous species were effectively removed by plasma etching (Figs. S-7C and S-8C). Concurring with the results of SIMS, the carbonaceous species on the surface were effectively removed

by plasma etching. Significant changes in the Si 2p spectra were observed on the SALDI surface due to plasma etching. The spectrum shape changes from largely metallic to oxides (Figs. S-7D and S-8D). The high-resolution Si 2p spectra was deconvoluted into three sets of peaks corresponding to elemental silicon, silicon dioxide and sub-oxides. Each pair of peaks corresponds to the lower and the higher spin of a chemical state. The literature value of Si 2p spin orbit splitting is 0.617 eV [28].

The oxide thickness, d_{oxide}, can be calculated from [29]

$$d_{oxide} = L_{SiO_2} \cos\theta \ln\left(1 + \frac{R_{exp}}{R_0}\right)$$

where L_{SiO_2} is the attenuation length for the Si 2p photoelectrons in SiO_2, and θ is the angle of emission of the detected electrons from the surface normal. R_{exp} is the measured Si 2p intensity ratio I_{SiO_2}/I_{Si} from the sample, and R_0 is the same ratio for signals from infinite solids with flat surfaces measured under identical conditions. Take the value $R_0 = 0.83$ and $L_{SiO_2} = 2.36$ nm. The calculated d_{oxide}(as-received) = 1.0 nm and d_{oxide}(plasma etched) = 2.8 nm.

3.5. Water contact angle (WCA) measurements

The WCA measurement gives information about the wettability of the surface, which directly influences the sample droplet aggregation and distribution and hence WCA measurement was carried out and the substrate S3 was used. The unmodified substrate was hydrophilic and had a WCA $25.1 \pm 0.8^\circ$. The substrate became hydrophobic after fluorosilane derivatization and had a WCA $92.3 \pm 2.0^\circ$. On the other hand, the removal of surface contamination and oxidation induced by argon plasma etching resulting in the surface became highly hydrophilic and had a WCA less than 10°. A smooth fluorosilanized Si/SiO_2 modified surface has been reported to having a WCA $\sim 109^\circ$ [30], and noticeably, the derivatized SALDI substrate exhibited a negative derivation from 109°.

Contact angle can also be considered in terms of the thermodynamics of the materials involved and provides information related to the interfacial free energies, which is in turned influenced by the surface morphology and chemistry. The classical works of Wenzel [31] and Cassie and Baxter [32] have established the relationship between the roughness and surface energy to the water wettability of rough or porous surface. Cassie and Baxter's model differs from Wenzel's in that a porous hydrophobic surface traps air in the hollows of the pores.

It was noted that in the surface morphology analysis, the addition of iodine greatly influences the process of PSi formation. The size of the surface nanostructures became smaller than those prepared by the standard anodization method did. The porosity of the substrates was also relatively low. The non-porous approach and the proposed reduction to the characteristic size of the surface irregularity for the SALDI substrates [7,23] actually shifts the system further away from Cassie/Baxter's system to an ideal Wenzel's system.

It is proposed that because of the surface morphology of the SALDI substrates, during the contact with a droplet of water, the surface exhibits a contact angle lower than 109°. By using the Wenzel's law, and taking $\theta_c = 93^\circ$, $\theta_1 = 109^\circ$, for the SALDI system, the calculated value of $r = 0.16$. This indicates that the increased surface area (in contact with water) was ~16%.

The enhanced surface area introduced by the surface roughness in the SALDI substrates makes the surface acquire an excess free surface energy and therefore the surface has strong interactions or adhesion to the adsorbate. The non-porous roughened morphology therefore increases gaseous adsorption and diffusion efficiency, which leads to an increase in ion current in the GC/SALDI-MS approach. Accordingly, the enhanced adsorption and diffusion is apparently required for the GC/SALDI-MS, in which the rate of gaseous adsorption of analyte is a significant determining factor. However, the opposite is required for the liquid deposition approach. A high WCA leads to the confinement of the analyte solution droplet into a smaller area during sample deposition and hence leads to a high LDI performance. This also prevents cross contamination due to sample droplet spreading. Lowering the surface free potential also reduces the rate of atmospheric species adsorption.

3.6. Investigation of the laser modification of the SALDI substrate by XPS and SIMS imaging

The GC/SALDI-MS approach requires a surface to be further "subjecting... to optical radiation in water [vapor] environment at intensity lower than destruction threshold of [the] surface" [19]. This process occurs inside the ion source, in the presence of residual water vapor and ablates materials that have already been adsorbed onto the surface and is referred to as surface activation [15]. The advance techniques of SIMS and XPS imaging were used to investigate the effects of laser etching or ablation of the SALDI substrates under this condition and reveal the full picture.

A laser-modified surface was first examined by SIMS ion mapping, in which a wide variety of molecular species was accessed with an improved lateral resolution relative to the XPS imaging technique. However, SIMS is surface specific and only the topmost layer was detected. Ion images were generated by a finely focused primary ion beam produced by Ga^+ liquid metal ion gun swept the sample in a raster pattern of an area $500\,\mu m \times 500\,\mu m$ and software saved secondary ion intensities as a function of beam position. Resolution was 512×512 pixels. Fig. 5A shows an optical image of the surface used for imaging. Three areas, corresponding to laser-modified region, non-modified region and a particle (appeared as a purple dot) are highlighted. After laser etching, a visual alternation can be seen and the laser-modified region appeared more reflective than the non-modified region.

The positive and negative ion SIMS images are shown in Fig. 5B and C, respectively. The images of H^+, CH_2^+, CH_3^+, O^- and OH^- ionic species were intense and were relatively uniform on the images. This suggests that these species might have been adsorbed subsequently onto the surface after the GC/SALDI experiment. On the other hand, ionic species of silicon oxides (SiO^+, SiO_2^-, SiO_3^-) and hydroxides ($SiHO^+$, $SiHO_2^-$, $SiHO_3^-$) were observed on the laser-modified region with higher intensities relative to the non-modified region. The ion intensity of the silicon hydride ions (SiH_2^+, SiH_3^+, SiH^-, SiH_2^-) were lower on the laser-modified region relative to the non-modified region. Similarly, Si^+ ion was intense and showed a higher intensity on the laser-modified region and yet the intensity of Si^- was lower on the same area. This observation pointed to the matrix effects caused by silicon oxides [33], and possibly involving other highly electronegative ions (F^-, Cl^-, I^-, O_2^-), and favor the formation of Si^+. Overall, the surface was oxidized during the GC/SALDI process and the observation was in coherence with that reported previously.

However, the ion intensity of SiH^+ was also higher on the modified region. Even if matrix effects had a role in enhancing the intensity of Si^+ on the modified region, this still could not explain the observed pattern of SiH^+. A possible explanation is that laser induced a further reaction with remaining etchant on the surface. This was supported by SiF^+, F^- and I^- images. In fact, halides ion such as fluorides, chloride and iodide (F^-, Cl^-, I^-) were higher on the laser-modified area relative to the non-modified area. The same was true for Na^+ and K^+. Indeed, the significant difference of F^- and I^- ion between the laser-modified and non-modified regions was noteworthy and did not support the view that Si–I was substituted by another functional group proposed previously but the halides became surface passivated, possibly in the form of Si–F and Si–I.

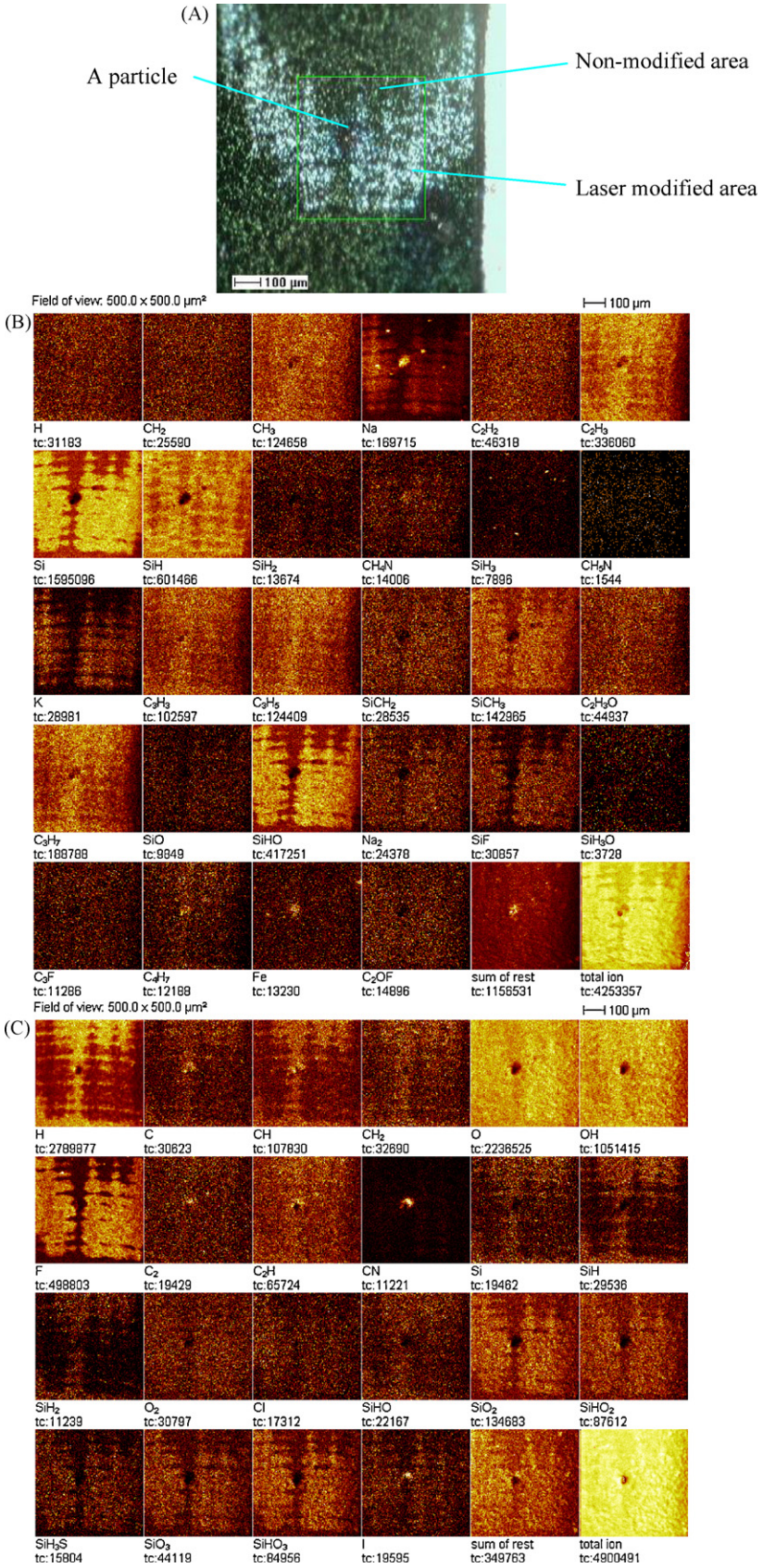

Fig. 5. (A) An optical image of a SALDI substrate after GC/SALDI-MS investigation. The square indicates the area used for SIMS imaging. (B and C) Positive and negative ToF-SIMS ion maps of a laser-modified SALDI surface. Logarithmic scaling and Poisson correction was used to scale the contrast of the images.

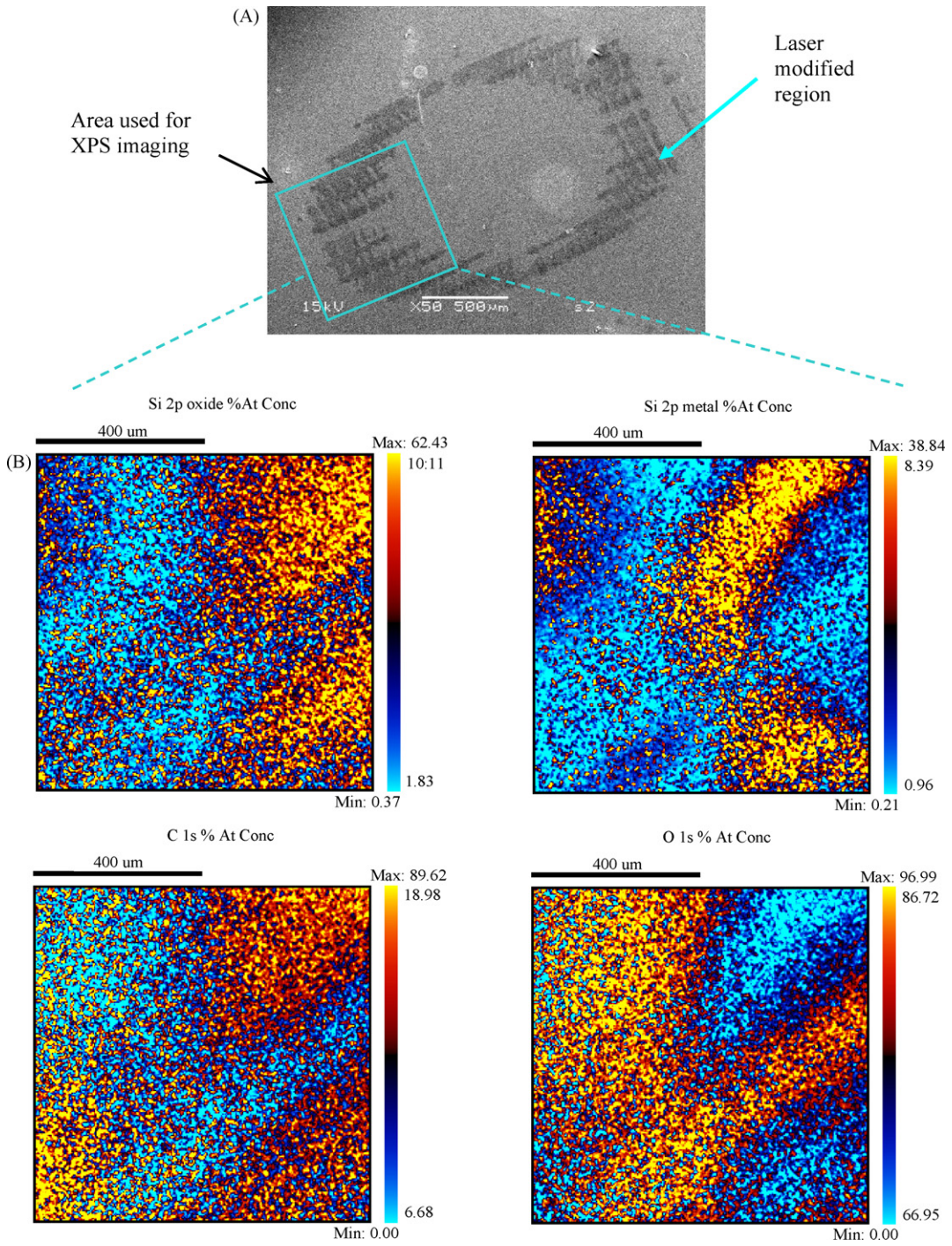

Fig. 6. (A) A SEM image of a SALDI substrate after GC/SALDI-MS investigation. An oval shaped burn mark is shown on the image. (B) XPS images of the same SALDI substrate that has been laser-modified.

On the other hand, the particle observed might be an organic salt, as species such as Na^+, Fe^+, CN^-, and I^- were relatively strong in this region.

A laser-modified substrate was further investigated by SEM (Fig. 6A). A ring was observed on the image. This ring was due to a circular movement of laser beam diverted by a rotating mirror during the GC/SALDI-MS investigation [15]. This region had thus been laser-modified under the GC/SALDI-MS condition and the surrounding area had not been modified by laser. The laser-modified ring appeared darker relative to its surrounding area. Furthermore, because it was the laser spot in rotation instead of the target stage transition, the laser incidence angle and spot size varied. Consequently, the thickness of the ring circumference varied and so would have the localized laser intensity and temperature during the GC/SALDI experiment.

The surface was studied by XPS chemical imaging analysis. Multi-spectral datasets were acquired at 0.2 eV intervals. Images were taken from an area of case 800 μm × 800 μm. Resolution was 256 × 256 pixels. The multi-spectral image data was then processed with SVD sorting and PCA. The final images were reconstructed from the first two principle components. Four images corresponding to silicon dioxide [Si 2p oxide], silicon element [Si 2p metal], carbon [C 1s] and oxygen [O 1s] are displayed (Fig. 6B).

Table 2
XPS imaging result summary.

Signal from in the modified region	Relative change in signal intensity from the non-modified region	Relative change in concentration from the non-modified region	Comment
Si/SiH	Increase	Increase	A combination of reduction of the oxide thickness and contamination over layer, and reaction with remaining etchant and/or H_2O, increase in density due to surface melting/reconfiguration. Consistent with the SIMS images of SiH^+, SiF^+, SiH_3S^-
SiO_xH_y	Increase	Increase	Further supported by O 1s and Si 2p XPS spectra shifts or broadens to the higher BE. Supported by the SIMS images of $SiHO^+$, $SiHO_2^-$, $SiHO_3^-$
SiO_x	Decrease	Total oxide thickness decrease	The total oxide layer thickness was reduced. However, the topmost surface oxide concentration increased and is supported by the SIMS images of SiO^+, SiO_2^-, SiO_3^-, and also Si^+, Na^+, K^+ (matrix effect)
C	Increase	Increase in covalent linked species	Contributed differently from different molecular species as indicated by XPS C 1s spectrum shifted to the higher BE (Fig. S-11). This is supported by the SIMS images of the increase of $SiCH_2^+$, $SiCH_3^+$, and decrease of $C_2H_3^+$, $C_3H_7^+$, C^-, CH^-, and CH_2^- on the modified region. Adsorbed organic species were partly washed off by solvent washing and consequently a high contrast in the image was displayed

The XPS images of Si 2p oxide and C 1s showed a very similar pattern and a higher intensity was observed on the right side of the image (laser-modified region) than the left side of the image (non-modified region). This suggests that silicon dioxide and carbide complexes could be by-products created during the SALDI process. This was in coherence with the SIMS ion mapping of the corresponding ions. The XPS images of Si 2p element and O 1s showed a higher Si element but lower oxygen signal on the laser-modified area relative to non-modified region. The pattern of O 1s signal was also a mirror image to that of Si 2p oxide and C 1s. Given the contraction of the O 1s and Si 2p image, XPS spectra were therefore reconstructed from the imaging data.

Si 2p core-level spectra were reconstructed by summing the multi-spectral datasets of the selected pixels of the Si 2p image, using the relative intensity of Si (element), which was corresponding to the laser-modified and non-modified regions of the surface (Fig. S-9). The spectra were deconvoluted to elemental Si and silicon oxides. The change in elemental Si and oxides intensity between the laser-modified and non-modified regions indicated a thinning of the oxide/hydroxide layer. O 1s core-level spectra were also reconstructed and were deconvoluted to SiO_2 and SiOH components (Fig. S-10). The reconstructed O 1s spectra showed that the laser-irradiated region had a higher proportion of SiOH but lower proportion of SiO_2. It is also important to note that the surface roughness also influences the path of the photoelectrons [34]. For that reason, apart from thinning of oxide thickness, a microscopic rearrangement of surface morphology due to laser ablation or surface melting must have occurred. The result of the XPS imaging as compared to the SIMS ion mapping is summarized in Table 2.

The significance of the SIMS and XPS imaging is that the result in part supports the proposition that the surface Si–OH moieties are a major proton source for the SALDI process. The proton exchange between the Si–OH moieties and the analyte resulted in SiO_x formation as proposed previously [15,23]. However, the proposed hydroxylation reaction that occurred may well be initiated by exciton and/or was thermal accelerated. There was no evidence to support the substitution of Si–I functional group by hydroxyl groups. Fluorine passivation to the SALDI substrates possibly occurred during the laser etching stage and no evidence obtained supporting this was produced during the chemical etching procedure. Consequently, the formation of dangling bonds due to the iodine dissociation and subsequently reaction with adsorbed water as proposed previously cannot be considered a viable process and the involvement of Si–I, or its dissociation is not required [23]. However, the thickness of the oxide layer becomes significantly reduced as a result of the intense heated induced by the laser radiation and could be just a few atomic layers thick during the laser etching process. The fluorine passivation might have another role such as acidifying the surface Si–OH moieties for efficient proton exchange. The situation is comparable to the fluorosilane derivatization where fluorine withdraws electron density from the surface Si–OH moieties and enhances the proton exchange efficiency and monolayer self-assembly during derivatization. Recrystallization of the melted silicon crystalline resulted in the final form of the surface detected by the SIMS and XPS imaging technique.

4. Conclusions

The latest development of SALDI substrate has taken the route to support the development of the novel gas-phase introduction interface of GC/SALDI mass spectrometer. Typical substrates received were non-porous or relatively smooth and had a surface roughness of a few nm. However, only the substrates that had a thick and dense nanostructure layer are effective for mass spectrometry application. From the observations as a whole, the LDI performance of substrates does not strongly depend on surface roughness, but perhaps more on the thickness, dimension and density of the surface nanostructures.

The use of a mild oxidizing etching electrolyte (the iodine-containing HF solution) in the preparation of the SALDI substrate generated an ultra-thin oxide layer on the silicon surface and the surface was therefore hydrophilic. It should note that the GC/SALDI-MS approach relies on enrichment of the analyte continuously adsorbed onto the surface to achieve high sensitivity. The surface is needed to be effective for adsorption and diffusion. Other reasons include contamination control because a porous surface is difficult

to clean. These issues have been paramount in the GC/SALDI-MS development and have over-shadowed the factors actually valid for enhancing LDI activity. However, the SALDI substrate optimized for GC/SALDI is actually counter productive for SALDI-MS using the conventional liquid deposition approach. It is because the physicochemical properties of the substrate lead to the rapid adsorption of atmospheric contamination, which leads to lowering of the mass resolution, production of background interference in the mass spectra and suppression of analyte desorption or ionization. Consequently, the SALDI substrates in their current form are considered not ideal for the purpose for biological mass spectometry.

Argon plasma etching approach was adopted to tackle the surface contamination of the SALDI substrates and aimed to improve its usability. Although argon plasma etching led to a clear silanol surface, the thickness of oxide layer was increased, making the surface more reflective to laser radiation and degrading the LDI performance. Therefore, the cleaned surfaces were further derivatized with fluorosilane. An ability to generate Si–OH intermediate essential for the self-assembly monolayer reaction and to clean the surface simultaneously is an advantage of this approach. The modified substrate showed some promise for biological mass spectrometry.

Although it is a reasonable deduction that a sub-surface state of silicon induced by laser etching is an essential part of the SALDI mechanism, there is still missing evidence to support this proposition. The investigation of laser modification by SIMS and XPS imaging has revealed the aspects of chemical change that had been previously omitted or misconceived and provides further insight of the SALDI ionization mechanism.

However, whether the surface is porous or not, highly roughened or not, chemically etched or not, some forms of ion could be produced. This indicates that the presence of pores or roughness on the surface is not an absolute requirement for LDI, but rather an enhancement or cofactor that assists ion formation. The same principle should therefore apply so as to whether the surface is etched by standard galvanostatic etching or anodization with addition of iodine etching additive, SALDI using gas-phase adsorption approach or liquid-disposition approach. The minimal requirement here is nanostructures on semiconductor substrate. It is known that when a particle has a size approaching or less than 100 nm, it often exhibits quantum properties which would otherwise not be observable on micron-size or larger particles. Since PSi is generally described as an assembly of nanocrystallites [35], it is possible that the nano-sized surface structures are directly implicated in the optical coupling or energy deposition required for the SALDI activity [36,37].

Acknowledgements

This work was supported by RSC/EPSRC research funding. The author thanks Frank Rutten for assistance with the SIMS work, Emily Smith for assistance with the XPS work and Nigel Halliday for providing the bacterial extract for investigation. The authors also thank Vladimir Karavanskii and Sergey Nikiforov for the preparation of the SALDI substrates in the investigation and the useful discussion. The author also thanks Dave Barrett and Morgan Alexander for their academic support during this study.

Appendix A. Supplementary data

Supplementary data associated with this article can be found, in the online version, at doi:10.1016/j.ijms.2009.12.003.

References

[1] M. Karas, F. Hillenkamp, Laser desorption ionization of proteins with molecular masses exceeding 10,000 daltons, Anal. Chem. 60 (1988) 2299–2301.
[2] K. Tanaka, H. Waki, Y. Ido, S. Akita, Y. Yoshida, T. Yoshida, Protein and polymer analyses up to *m/z* 100,000 by laser ionization time-of-flight mass spectrometry, Rapid Commun. Mass Spectrom. 2 (1988) 151–153.
[3] C. Afonso, N. Budimir, F. Fournier, J.-C. Tabet, Activated surfaces for laser desorption mass spectrometry: application for peptide and protein analysis, Curr. Pharm. Des. 11 (2005) 2559–2576.
[4] A.M. Dattelbaum, S. Iyer, Surface-assisted laser desorption/ionization mass spectrometry, Expert Rev. Proteomics 3 (2006) 153–161.
[5] Z. Guo, A. Ganawi, Q. Liu, L. He, Nanomaterials in mass spectrometry ionization and prospects for biological application, Anal. Bioanal. Chem. 384 (2006) 584–592.
[6] J. Sunner, E. Dratz, Y.-C. Chen, Graphite surface-assisted laser desorption/ionization time-of-flight mass spectrometry of peptides and proteins from liquid solutions, Anal. Chem. 67 (1995) 4335–4342.
[7] S. Alimpiev, S. Nikiforov, V. Karavanskii, T. Minton, J. Sunner, On the mechanism of laser-induced desorption-ionisaqtion of organic compounds from etched silicon and carbon surfaces, J. Chem. Phys. 115 (2001) 1891–1901.
[8] Y. Wada, T. Yanagishita, H. Masuda, Ordered porous alumina geometries and surface metals for surface-assisted laser desorption/ionization of biomolecules: possible mechanistic implications of metal surface melting, Anal. Chem. 79 (2007) 9122–9127.
[9] H. Sato, T. Seino, A. Yamamoto, M. Torimura, H. Tao, Soft laser desorption/ionization mass spectrometry using a pyroelectric ceramic plate, Chem. Lett. 34 (2005) 1178–1179.
[10] J. Wei, J. Buriak, G. Siuzdak, Desorption/ionization mass spectrometry on porous silicon, Nature 399 (1999) 243–246.
[11] O. Bisi, S. Ossicini, L. Pavesi, Porous silicon: a quantum sponge structure for silicon based optoelectronics, Surf. Sci. Rep. 38 (2000) 1–126.
[12] H. Föll, M. Christophersen, J. Carstensen, G. Hasse, Formation and application of porous silicon, Mater. Sci. Eng. R 39 (2002) 93–141.
[13] V.P. Parkhutika, E. Matveeva, Observation of new oscillatory phenomena during the electrochemical anodization of silicon, Electrochem. Solid State Lett. 2 (1999) 371–374.
[14] M. Christophersen, J. Carstensen, H. Föll, Macropore formation on highly doped n-type silicon, Phys. State Solidi (a) 182 (2000) 45–50.
[15] S. Alimpiev, A. Grechnikov, J. Sunner, V. Karavanskii, Y. Simanovsky, S. Zhabin, S. Nikiforov, On the role of defects and surface chemistry for surface-assisted laser desorption ionization from silicon, J. Chem. Phys. 128 (2008) 014711–014719.
[16] S. Alimpiev, A. Grechnikov, J. Sunner, A. Borodkov, V.A. Karavanskii, Y. Simanovsky, S. Nikiforov, Gas Chromatography/Surface-Assisted Laser Desorption Ionization Mass Spectrometry of Amphetamine-like Compounds, Anal. Chem. 81 (2009) 1255–1261.
[17] T.V. Voloshina, T.N. Zavaritskaya, I.V. Kavetskaya, V.A. Karavanskii, D.A. Romashov, Formation and photoluminescence properties of porous silicon produced in iodine-containing electrolytes, J. Appl. Spectrosc. 69 (2002) 275–278.
[18] T.V. Voloshina, I.V. Kavetskaya, V.A. Karavanskii, Influence of iodine-containing solutions on the condition of a porous silicon surface and its photoluminescent properties, J. Appl. Spectrosc. 71 (2004) 89–93.
[19] Alimpiev, S.S., Nikiforov, S.M., Grechnikov, A.A., Karavanskii, V.A., Sunner, J.A., Method of forming of rough surface of silicon substrates and electrolyte for anode etching of silicon substrate, Russia Patent. RU 2003-101425, RU 2217840 (2003).
[20] V. Karavanskii, W. Gillin, A. Sapelkin, N.N. Melnik, T.N. Zavaritskaya, Photoluminescence relaxation kinetics in vapor etched porous silicon, in: Proceedings of the SPIE International Conference on Advanced Laser Technologies, vol. 6344, Tianjin, China, 2005, pp. 286–292.
[21] Z. Shen, J.J. Thomas, C. Averbuj, K.M. Broo, M. Engelhard, J.E. Crowell, M.G. Finn, G. Siuzdak, Porous silicon as a versatile platform for laser desorption/ionization mass spectrometry, Anal. Chem. 73 (2001) 612–619.
[22] W. Lewis, Z. Shen, M.G. Finn, G. Siuzdak, Desorption/ionization on silicon (DIOS) mass spectrometry: background and applications, Int. J. Mass Spectrom. 226 (2003) 107–116.
[23] S.S. Alimpiev, S.M. Nikiforov, A.A. Grechnikov, J.A. Sunner, Novel technique for ultra sensitive detection of organic compounds, in: NATO Science Series. II: Mathematics, Physics and Chemistry, Kluwer Academic Publishers, 2004, pp. 101–112.
[24] R.A. Kruse, X. Li, P.W. Bohn, J.V. Sweedler, Experimenetal factor controlling analyte ion generation in laser desorption/ionization mass spectrometry on porous silicon, Anal. Chem. 73 (2001) 3639–3645.
[25] Q. Zhang, H. Zou, Z. Guo, Q. Zhang, X. Chen, J. Ni, Matrix-assisted laser desorption/ionization mass spectrometry using porous silicon and silica gel as matrix, Rapid Commun. Mass Spectrom. 15 (2001) 217–223.
[26] H. Sato, A. Nemoto, A. Yamamoto, H. Tao, Surface cleaning of germanium nanodot ionization substrate for surface-assisted laser desorption/ionization mass spectrometry, Rapid Commun. Mass Spectrom. 23 (2009) 603–610.
[27] T. Kinumi, Y. Shimomae, R. Arakawa, Y. Tatsu, Y. Shigeri, N. Yumoto, E. Niki, Effective detection of peptides containing cysteine sulfonic acid using matrix-assisted laser desorption/ionization and laser desorption/ionization on porous silicon mass spectrometry, J. Mass Spectrom. 41 (2006) 103–112.
[28] H.W. Nesbitt, G.M. Bancroft, R. Davidson, N.S. McLntyre, A.R. Pratt, Minimum XPS core-level line widths of insulators, including silicate minerals, Am. Mineral. 89 (2004) 878–882.

[29] M.P. Seah, S.J. Spencer, Ultrathin SiO_2 on Si II. Issues in quantification of the oxide thickness, Surf. Interface Anal. 33 (2002) 640–652.
[30] Y. Coffinier, S. Janel, A. Addad, R. Blossey, L. Gengembre, E. Payen, R. Boukherroub, Preparation of Superhydrophobic Silicon Oxide Nanowire Surfaces, Langmuir 23 (2007) 1608–1611.
[31] R.N. Wendel, Resistance of solid surfaces to wetting by water, J. Ind. Eng. Chem. 28 (1936) 988–994.
[32] A.B.D. Cassie, S. Baxter, Wettability of porous surfaces, Trans. Faraday Soc. 40 (1944) 546–551.
[33] K. Mann, M.L. Yu, Effect of chemical bonding on positive secondary-ion yields in sputtering, Phys. Rev. B 35 (1987) 6043–6050.
[34] P.L.J. Gunter, O.L.J. Gijzeman, J.W. Niemantsverdriet, Surface roughness effects in quantitative XPS: magic angle for determining overlayer thickness, Appl. Surf. Sci. 115 (1997) 342–346.
[35] L. Canham, Properties of Porous Silicon, Institution of Engineering and Technology, Stevenage, 1997.
[36] J.D. Cuiffi, D.J. Hayes, S.J. Fonash, K.N. Brown, A.D. Jones, Desorption-ionization mass spectrometry using deposited nanostructured silicon films, Anal. Chem. 73 (2001) 1292–1295.
[37] A. Vertes, Soft laser desorption ionization—MALDI, DIOS and nanostructures, in: C.R. Phipps (Ed.), Laser Ablation and its Applications, Springer, 2007, pp. 505–528.